Improved navigation-based motion compensation for LFMCW synthetic aperture radar imaging

Jamal Saeedi & Seyed Mohammad Alavi

VOLUME 9   ISSUE 3   MARCH 2015

ONLINE FIRST

Signal, Image and Video Processing

🜨 Springer

🜨 Springer

Springer

ORIGINAL PAPER

Improved navigation-based motion compensation for LFMCW synthetic aperture radar imaging

Jamal Saeedi · Seyed Mohammad Alavi

Abstract In this paper, a new motion compensation algorithm using navigation data is proposed for frequency domain algorithm of synthetic aperture radar (SAR) imaging. SAR processing method assumes that the sensor is moving in a straight line at a constant speed; however in reality, a SAR platform will deviate from this ideal. This non-ideal motion can seriously degrade the SAR image quality. In this study, the linear frequency-modulated continuous wave SAR signal model is presented. The effects of non-ideal motion during the SAR signal modeling are investigated, and new method for motion correction is developed. This new motion compensation algorithm is verified with simulated data and with actual data collected using FMCW mode SAR dataset.

Keywords Synthetic aperture radar · Motion compensation · Frequency-modulated continuous wave · Strip-map

1 Introduction

Synthetic aperture radar (SAR) processing algorithms (without any phase error correction or motion compensation step) assume that the radar platform moves at a constant speed in a straight trajectory. Nevertheless, this is not true as the platform experiences a variety of deviations from the ideal path in actual data collection. These deviations happen when the platform changes its attitude, speed, or is subjected to turbulence in the atmosphere. Variations in along-track ground speed result in non-uniform spacing of the radar pulses on the ground. This non-uniform sampling of the Doppler spectrum results in erroneous calculations of the Doppler phase history. Changes in pitch, roll, and yaw introduce errors of a different kind. The pitching displaces the antenna footprint on the ground, the roll changes the antenna gain pattern over the target area, and the yaw introduces a squint. Pitch and yaw shift the Doppler centroid, with the shift being range dependent in the yaw case. Translational motion causes platform displacement from the nominal, ideal path. This results in the target scene changing in range during data collection. This range shift also causes inconsistencies in the target phase history. These deviations introduce errors in the stored data, which lower SAR image quality.

In this paper, we have only considered translational motion error in the SAR signal modeling. Coherent processing of SAR data requires precise knowledge of the relative geometric between the flight trajectory and the scene being imaged. This geometry information is typically acquired using navigation systems such as inertial measurement units (IMUs) [1] and global positioning system (GPS) receivers [2]. In a typical SAR system, navigation data are employed for motion compensation (MC) [3,4].

Constructions of very small SAR systems are possible by using a linear frequency-modulated continuous wave (LFMCW) signal in the radar transmitter [5–10]. Combined with an analog de-chirp in the receiver, these systems can be made with hardware which is simpler, cheaper, and consumes less power than conventional pulsed SAR systems. This enables the use of low cost SARs on small unmanned aircraft systems (UAS) [8]. The motion error problem is particularly apparent to the UAS SAR, because it is easily disturbed by the atmospheric turbulence due to its small size

J. Saeedi (✉)
Department of Electrical Engineering, Amirkabir University of Technology (Tehran Polytechnic), 424, Hafez Ave., Tehran, Iran
e-mail: jamal.saeedi@yahoo.com

S. M. Alavi
Department of Electrical Engineering, Imam Hossein Comprehensive University, Babaei Hwy, Tehran, Iran
e-mail: malavi@ihu.ac.ir

and lightweight. Therefore, for the UAS SAR imaging, MC strategies are important and advisable. For this reason, we have considered SAR in LFMCW mode for theoretical discussions; however, it can be generalized for pulsed mode SAR.

In this study, a complete FMCW SAR signal model is developed, which takes into account the effect of the motion during the chirp. In addition, an improved motion compensation algorithm using navigation data is proposed which works for the FMCW SAR data [5–10]. MC algorithms for traditional pulsed mode SAR have been extensively studied [4,11]; however, it is a challenge to extend them for FMCW mode SAR signal. In pulsed mode SAR, the platform is assumed to be stationary during each pulse, and the motion takes place between pulses (start-and-stop approximation). In contrast, in FMCW mode SAR, the signal is continuously being transmitted and received; therefore, the motion takes place during the chirp.

There are three different errors caused by motion in FMCW SAR data. The first error is because of the motion during the chirp. The second error is the phase error caused by translational motion of the platform. The last error is range shift introduced by translational motion. In the traditional two-step motion compensation algorithm [4], the second error is only considered for compensation. In [12], Zaugg and Long proposed a new MC method, which uses a two-step phase compensation with modified phase function compared to the traditional method [4]. Similar to traditional MC algorithm only the second type of error is considered for compensation. Wang et al. [13] used a similar two-step compensation applying in omega-k algorithm for FMCW data. However, motion during chirp and the shift error are not considered in the algorithm. The results of MC algorithm for Ka-band airborne FMCW SAR are provided by Meta et al. [14]; however, the theoretical treatment of MC algorithm is not mentioned in the paper.

This paper presents the development of a new MC algorithm that is appropriate for use with frequency domain image formation methods like range-Doppler algorithm (RDA), which also accounts for the motion during the chirp. Specifically, we have proposed a new MC algorithm, which considered all of the errors caused by motion in the FMCW SAR data.

The remainder of this paper is organized as follows. The fundamental of SAR signal processing in LFMCW mode is briefly reviewed in Sect. 2. Section 3 gives the description of the proposed MC algorithm using navigation data. Section 4 illustrates experimental results in which a SAR system images a few point targets with non-ideal motion. The known deviations are used to compensate for the effects of non-ideal motion in the simulated data. A numerical analysis of the simulation results is performed, which compares the proposed MC algorithm to the traditional method [4]. The developed algorithm is applied to actual data from SAR system in LFMCW mode, and the results are presented. Finally, conclusions are given in Sect. 5.

2 LFMCW synthetic aperture radar signal processing

In this section, first we will describe how to model the transmitted and received signal based on LFMCW waveform. Then, signal processing algorithm for image formation of received SAR signal is explained. SAR system illuminates the scene with a series of coherent pulses while passing by a target. The series of radar echoes from the target area are digitized and processed to form the image.

Before the SAR signal is generated, a number of important system parameters should be determined, including carrier frequency, bandwidth, pulse length, and pulse repetition frequency (PRF). The transmitted signal is a LFM waveform, where the signal spans the bandwidth over the pulse length. This cycle is repeated at the PRF. The SAR signal is usually generated at or near baseband and then mixed up to the desired operating frequency before transmission. The LFM transmit signal can be expressed as:

$$s_t(t) = A(t) \exp\left(j \left(2\pi f_0 t + \pi k_r t^2 + \varphi_0 \right) \right) \qquad (1)$$

where $A(t)$ is the signal amplitude as a function of time t and defines the pulse length with a rect function, k_r is the chirp rate, f_0 is the frequency at the beginning of the chirp, and φ_0 is the starting phase which can usually be neglected.

In the transmission chain, a power amplifier increases the power to a specified level. The amplified signal transmitted through the antenna propagates to the target area. A very small portion of the transmit signal is reflected back to the radar. By neglecting the time-scaling influences on the pulse envelope, the echoed signal from target can be expressed as:

$$s_r(t, \eta) = A'(t) \exp\left(j \left(2\pi f_0 (t - \tau) + \pi k_r (t-\tau)^2 + \varphi_0 \right) \right) \qquad (2)$$

where t is fast time, η is slow time (or azimuth time), and $A'(t)$ is an attenuated version of $A(t)$ and τ is the two-way time of flight to the target at range R.

In the pulsed mode, the pulse duration is short about a few microseconds; however, for the LFMCW mode, the pulse duration is about milliseconds, corresponding to the pulse repetition interval. Therefore, the number of samples for LFMCW mode could be too many. The de-chirp-on-receive technology is generally used in the LFMCW SAR system to reduce the sampling requirements and data rate [15,16].

With an analog de-chirp, the received signal is mixed with a copy of the transmit signal and low-pass-filtered in hardware, which is mathematically equivalent to multiplying (1) by the complex conjugate of (2). This results in the de-chirped signal:

$$s_{dc}(t, \eta) = s_t \cdot s_r^* = A''(t)$$
$$\times \exp\left(j\left(2\pi f_0\tau + 2\pi k_r t \cdot \tau - \pi k_r \tau^2\right)\right) \quad (3)$$

SAR systems digitize this data and either store it on board, transmit it to a ground station, or process it on board. The last exponential term of (3) is well known as the residual video phase (RVP) [16]. Removing the RVP needs Fourier transformation (FT), phase multiplication, and inverse FT [16]. For range compression of de-chirped LFM signal, only one FT is necessary [17]. Assuming no motion during the chirp is equivalent to assuming R is not a function of t. Thus, the range-compressed signal is obtained using the following:

$$s_{rc}(f_r, \eta) = \int_\tau^{\tau+T} s_{dc}(t, \eta) \cdot \exp\left(-j2\pi f_r t\right) dt$$
$$= T \cdot \operatorname{sinc}\left(T\left(f_r - k_r\tau\right)\right)$$
$$\cdot \exp\left(j\pi \begin{pmatrix} k_r\tau \cdot T - f_r T + \\ k_r\tau^2 + 2f_0\tau - 2f_r\tau \end{pmatrix}\right) \quad (4)$$

where T is pulse width and f_r is frequency in range direction. From (4), we can see that the RVP term $\exp\left(-j\pi k_r \cdot \tau^2\right)$ has been removed after FT. Since the peak value of the range-compressed signal lies on $f_r = k_r \cdot \tau$, (4) can be simplified as follows:

$$s_{rc}(f_r, \eta) \approx T \cdot \operatorname{sinc}\left(T\left(f_r - k_r\tau\right)\right) \cdot \exp\left(j\pi\left(2f_0\tau - f_r\tau\right)\right) \quad (5)$$

In (5), there are two parts of phase item: one is the Doppler item, which is necessary for azimuth focusing, and the second part is slope factor, which is not only affecting adding window in range, but also impacting the azimuth focusing. Thus, it must be compensated before azimuth compression. Let the de-sloping factor be:

$$\varphi_{ds}(f_r, \eta) = \exp\left(j\pi f_r\tau\right) \quad (6)$$

From (6), the de-sloping factor is linear with τ, which means different compensation should be done with different slant range. However, the signal in range frequency domain is a Sinc function with very narrow width, and the peak value lies on $f_r = k_r \cdot \tau$, so, the de-sloping factor can be written as [16]:

$$\varphi_{ds}(f_r, \eta) \approx \exp\left(j\pi f_r^2/k_r\right) \quad (7)$$

Multiplying (5) by (7) then transforming inversely to range time domain, the range de-sloping is finished.

$$s_{ds}(t, \eta) \approx \int_0^\infty T \cdot \operatorname{sinc}\left(T\left(f_r - k_r\tau\right)\right) \cdot \exp\left(j2\pi f_0\tau\right)$$
$$\cdot \exp\left(j2\pi f_r t\right) df_r \approx \exp\left(j2\pi f_0\tau\right)\exp\left(j2\pi k_r \cdot t \cdot \tau\right) \quad (8)$$

After de-sloping, the range compression can be accomplished by adding window and performing FT in range direction.

Performing the time–frequency substitution of $f_r = k_r \cdot t$, the new range-compressed signal is obtained as follows:

$$s_{rc}(f_r, \eta) \approx \exp\left(j2\pi \cdot \tau \cdot (f_r + f_0)\right) \quad (9)$$

We approximate the FT using the principle of stationary phase (POSP), which is valid except in the extreme case of having radar frequencies very close to zero. An expression for the signal phase after the azimuth FT is computed by adding the phase term $-2\pi f_a\eta$ to (9), where η is azimuth frequency:

$$\phi = 2\pi \cdot \tau \cdot (f_r + f_0) - 2\pi f_a\eta$$
$$= \frac{4\pi}{c} \cdot R(\eta)(f_r + f_0) - 2\pi f_a\eta \quad (10)$$

where

$$R(\eta) = \sqrt{r_0^2 + (v \cdot \eta - x_0)^2} \quad (11)$$

Take the derivative of the phase with respect to η and solve for η at the point where the phase is stationary (i.e., where $d\phi/d\eta = 0$). Substitute obtained η into (10) and simplify to obtain the signal phase after the azimuth FT. The exponential that makes up the signal in 2D frequency domain can be expressed as:

$$s_{2d}(f_r, f_a) \approx \exp\left(-j\left(\frac{2\pi \cdot r_0}{v \cdot c}\sqrt{-f_a^2c^2 + 4(f_r + f_0)^2 v^2}\right.\right.$$
$$\left.\left. + \frac{2\pi \cdot f_a \cdot x_0}{v}\right)\right) \quad (12)$$

2.1 Considering motion during the chirp

Classical SAR imaging algorithms that use the start-and-stop approximation need to be modified for LFMCW SAR image processing. In order to explore what happens when we include the motion during the chirp, we assume that the platform motion is linear, calculate the two-way time of flight to a target τ, and approximate the change in range as linear during a single chirp; thus, using first-order Taylor approximation, we can obtain the following:

$$\tau = \frac{2 \cdot R(t, \eta)}{c} = \frac{2 \cdot \sqrt{r_0^2 + (v \cdot (t + \eta) - x_0)^2}}{c}$$
$$\approx \frac{2 \cdot R(\eta)}{c} + \frac{2 \cdot v \cdot (v \cdot \eta - x_0)}{c \cdot R(\eta)} \cdot t \quad (13)$$

where t is fast time, η is slow time (or azimuth time), τ is the two-way time of flight to the target at range R, and $R(\eta)$ is obtained using (11).

Substituting the approximation in (13) for τ in (3) and rearranging the terms yield [18]:

$$s_{dc}'(t, \eta) = s_{dc}(t, \eta) \cdot \exp\left(j\varphi_m(t, \eta)\right) \quad (14)$$
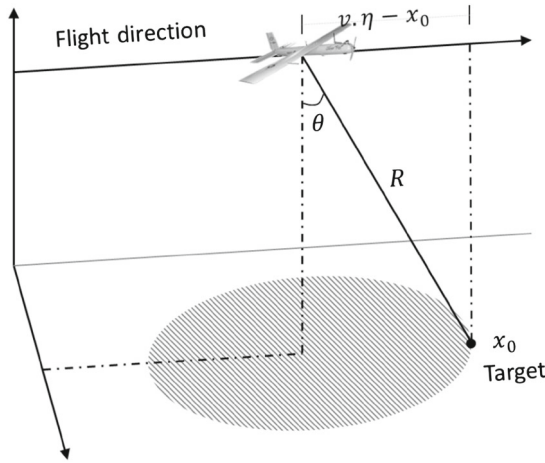
Fig. 1 SAR imaging geometry, the SAR flies to the right following the *arrow*. A target at range R is at a squint angle of θ

where $s_{dc}(t, \eta)$ is obtained using (3) and $\varphi_m(t, \eta)$ is obtained using the following:

$$\varphi_m(t, \eta) = \left(-\frac{8 \cdot v \cdot \pi \cdot k_r (v\eta - x_0)}{c^2} + \frac{4 \cdot v \cdot \pi \cdot f_0 \cdot (v\eta - x_0)}{R(\eta) \cdot c}\right) t$$
$$+ \left(-\frac{4 \cdot v^2 \cdot \pi \cdot k_r (v\eta - x_0)^2}{R(\eta)^2 \cdot c^2} + \frac{4 \cdot v \cdot \pi \cdot k_r \cdot (v\eta - x_0)}{R(\eta) \cdot c}\right) t^2$$
$$(15)$$

The effects of continuous motion on the signal phase can be seen by checking (15). As the range to target changes during a chirp, a change in frequency is introduced. The t^2 terms represent this chirp caused by the platform motion. The FT of this chirp is rect-like, and when convolved with (3) results in a spreading of the impulse response [18]. The motion also makes an effect on the carrier frequency, visible in the t terms. Additional insight can be obtained by observing that the final term is the Doppler frequency. Using the geometry of Fig. 1, the Doppler frequency is:

$$2\pi f_d = 2\pi \frac{2v \cdot \sin(\theta)}{\lambda} = 2\pi \cdot 2v \cdot \frac{(v\eta - x_0) f_0}{R(\eta) \cdot c} \quad (16)$$

The second t term in (15) is much larger than all the other terms and is the dominate effect of the platform motion which is a frequency shift equal to the Doppler frequency. This term translates into a range shift in the range-compressed data.

$$s'_{rc}(f_r, \eta) = \int_{\tau}^{\tau+T} s'_{dc}(t, \eta) \cdot \exp(-j2\pi f_r t) \, dt$$
$$= T \cdot \text{sinc}(T(f_r - k_r\tau + f_d))$$
$$\cdot \exp\left(j\pi \left(k_r\tau \cdot T - f_rT + k_r\tau^2 + 2f_0\tau - 2f_r\tau\right)\right)$$
$$(17)$$

Therefore, it should be compensated before range compression. The signal in time domain after RVP removal and including the effect of motion during the chirp can be expressed as:

$$s'_{dc}(t, \eta) = A''(t) \exp(j(2\pi f_0\tau + 2\pi k_r t \cdot \tau + 2\pi f_d t)) \quad (18)$$

Performing the time–frequency substitution of $f_r = k_r \cdot t$, and using the POSP, the signal in 2D frequency domain is obtained as follows:

$$s'_{2d}(f_r, f_a) \approx \exp\left(-j\left(\frac{2\pi \cdot r_0}{v \cdot c}\sqrt{-f_a^2 c^2 + 4(f_r + f_0)^2 v^2}\right.\right.$$
$$\left.\left. + \frac{2\pi \cdot f_a \cdot x_0}{v} - \frac{2\pi f_a f_r}{k_r}\right)\right)$$
$$(19)$$

where f_d is equal to azimuth frequency f_a.

The effects of the continuous platform motion can be removed at this point by multiplying (19) by the following phase function:

$$\varphi_{corr}(f_r, f_a) \approx \exp\left(-j\frac{2\pi f_a f_r}{k_r}\right) \quad (20)$$

Therefore, removing this effect needs an FT in azimuth direction, a phase multiplication, and an inverse FFT.

2.2 Frequency domain signal processing algorithm

The most frequently used algorithm for SAR signal processing is the range-Doppler algorithm (RDA) [19]. It was developed for processing SEASAT SAR data in 1978. There are three main steps to correctly focus the data using RDA: range compression, range cell migration correction, and azimuth compression.

3 Motion compensation using navigation data

The SAR processing method described in Sect. 2 assume that the platform moves at a constant speed in a straight line. Translational motion causes a platform displacement from the nominal, ideal path as shown in Fig. 2a. This results in the target scene changing in range during data collection. This range shift also causes inconsistencies in the target phase history. A target at range R_0 measured at range $R = R_0 + \Delta R_0$ results in a phase error in de-chirped signal (3) as:

$$s_{\Delta dc}(t, \eta) = A''(t) \exp(j(2\pi f_0(\tau_0 + \Delta\tau_0)$$
$$+ 2\pi k_r t \cdot (\tau_0 + \Delta\tau_0) - \pi k_r(\tau_0 + \Delta\tau_0)^2)) \quad (21)$$

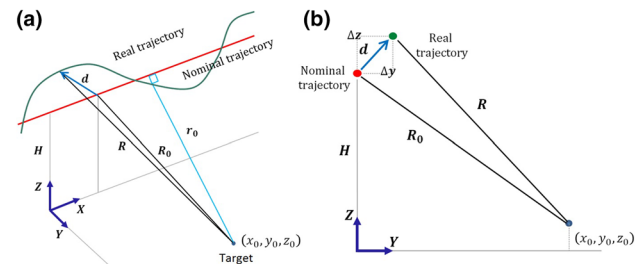where $\tau_0 = 2R_0/c$, and $\Delta\tau_0 = 2\Delta R_0/c$.

Fig. 2 **a** SAR geometry, **b** normal plane of the ideal trajectory

3.1 Flight trajectory estimation using GPS data

The motion errors can be compensated if the platform motion is measured using an on-board INS/GPS sensor. Using the

$$R(\eta; x_0, y_0, z_0) = \sqrt{(v \cdot \eta + \Delta x(\eta) - x_0)^2 + (\Delta y(\eta) - y_0)^2 + (H + \Delta z(\eta) - z_0)^2}$$
$$= R_0(\eta; x_0, y_0, z_0) + \Delta R_0(\eta; x_0, y_0, z_0) \tag{23}$$

GPS to Cartesian transform, we can find the real trajectory of SAR platform. The flight trajectory obtained by GPS to Cartesian transform has two evident problems: (1) fluctuations of flight trajectory because of GPS error and (2) altitude bias, because the height information is relative to sea level. These two problems should be resolved for MC. A common and completely reasonable response in selecting an interpolation strategy for improving motion data is to use the following:

$$C(t) = A_0 + A_1 t + A_2 t^2 + A_3 t^3 + \cdots + A_N t^N \tag{22}$$

a simple polynomial as the analytic function approximating the data in the interpolator [2]. Here, C represents the X, Y, or Z coordinate value, t is time, and A_0 through A_N are the coefficients of the polynomial, which are adjusted to fit the measured motion data.

The values of the coefficients will be determined by fitting the polynomial to the source data. This can be done by minimizing an error function that measures the misfit between the $C(t)$, for any given value of A, and the source data points. One simple choice of error function, which is widely used, is given by the sum of the squares of the errors.

In addition to polynomial fitting, we have used nadir return to improve the height estimation and remove GPS altitude bias. The platform height can be accurately estimated from the range-compressed SAR data. The nadir echo is evident in the range-compressed data, because there is no return signal for slant ranges shorter than the platform height or nadir. In the following, the theoretical treatment of full MC using navigation data for RDA is described.

3.2 Full motion compensation using flight trajectory information

For time domain reconstruction algorithms including time domain correlation (TDC) and back projection (BP), we can directly use the motion data to compensate the phase error. Here, the strip-map SAR geometry of Fig. 2a is assumed. The instantaneous motion error vector d, defined by the displacement between the real and nominal trajectories, is $[\Delta x(\eta), \Delta y(\eta), \Delta z(\eta)]$, where $\Delta y(\eta)$ and $\Delta z(\eta)$ represent

the cross-track displacement as shown in Fig. 2b. Knowing the coordinates of target (x_0, y_0, z_0), the real trajectory, and the nominal trajectory, the distances R and R_0 can be calculated from geometry:

$$R_0(\eta; x_0, y_0, z_0) = \sqrt{(v \cdot \eta - x_0)^2 + y_0^2 + (H - z_0)^2} \tag{24}$$

However, for frequency domain algorithms, it is not possible to directly use the motion data for phase error correction. The traditional MC method for RDA involves two steps [4]. First, the corrections are calculated for a reference range, R_{ref}, usually in the center of the swath. The first step of phase correction is as:

$$H_{\text{mc}_1} = \exp(-j2\pi f_0 \Delta \tau_{\text{ref}}) \tag{25}$$

where $\Delta \tau_{\text{ref}} = 2\Delta R_{\text{ref}}/c$. Then, the SAR data is range-compressed. This is the center-beam approximation [19] and is used in many MC algorithms. A second-order correction is applied to each range, according to the differential correction from the reference range. For each R, ΔR is calculated and the correction is formed as:

$$H_{\text{mc}_2} = \exp(-j2\pi f_0(\Delta \tau_0 - \Delta \tau_{\text{ref}})) \tag{26}$$

As we have mentioned in Sect. 1, translational motion introduces two type of error in the FMCW data. The first one is phase error in phase history of recorded SAR data, and the second one is range shift after range compression. The traditional MC method tries to compensate the first type of error using two-step correction filters. However, the correction filters in not accurately estimated based on FMCW SAR data as shown later. In addition, it ignores the range shift after range compression. Therefore, this method is not acceptable for a high-resolution SAR system

In this study, an efficient MC method is proposed to apply on the range-compressed data. Block diagram of the proposed MC algorithm incorporating with RDA is shown in Fig. 3. Correction of the effect of motion during chirp is considered as first step of motion compensation, which is explained in Sect. 2.1. In the following, the remaining steps for motion compensation are described. The range-compressed signal of (21) can be obtained using FT as follows:

$$s_{\Delta \text{rc}}(f_r, \eta) \approx T \cdot \text{sinc}(T(f_r - k_r(\tau_0 + \Delta \tau_0)))$$
$$\cdot \exp(j\pi(2f_0(\tau_0 + \Delta \tau_0) - f_r(\tau_0 + \Delta \tau_0))) \tag{27}$$
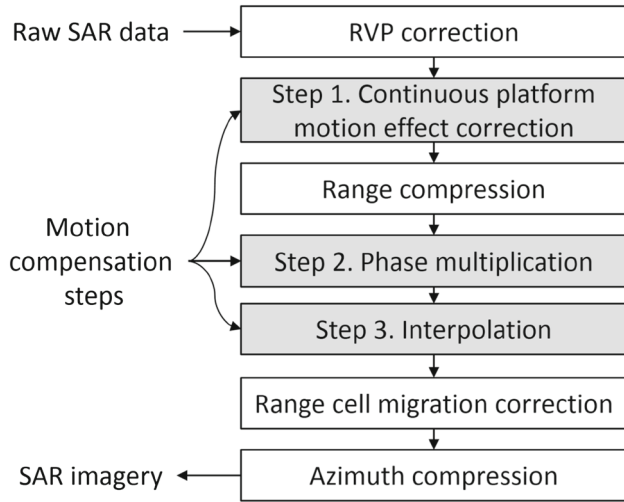
Fig. 3 Flowchart of the proposed MC algorithm incorporating with RDA

Since the peak value of the range-compressed signal lies on $f_r = k_r \cdot (\tau_0 + \Delta\tau_0)$, (27) can be simplified as follows:

$$s_{\Delta rc}(f_r, \eta) \approx T \cdot \text{sinc}(T(f_r - k_r(\tau_0 + \Delta\tau_0)))$$
$$\cdot \exp\left(j\pi\left(2f_0(\tau_0 + \Delta\tau_0) - k_r(\tau_0 + \Delta\tau_0)^2\right)\right) \quad (28)$$

From (28), we can find a correction filter, which works on the range-compressed data as:

$$H_{mc}(f_r, \eta) = \exp\left(j\pi\left(-2f_0\Delta\tau_0 + k_r\Delta\tau_0^2 + 2k_r\tau_0\Delta\tau_0\right)\right) \quad (29)$$

After the filtering, the range-compressed data become:

$$s_{\Delta rc}(f_r, \eta) \approx T \cdot \text{sinc}(T(f_r - k_r(\tau_0 + \Delta\tau_0)))$$
$$\cdot \exp\left(j\pi\left(2f_0\tau_0 - k_r\tau_0^2\right)\right) \quad (30)$$

Therefore, for the proposed method, there is no remaining phase error after phase correction. For exactly focusing the data, an azimuth-dependent interpolation should be used to compensate the range shift due to motion error. This is similar to the Stolt interpolation applied in omega-k algorithm [20]. The interpolation is defined as:

$$f_r - k_r(\tau_0 + \Delta\tau_0) \to f_r' - k_r\tau_0 \quad (31)$$

To achieve perfect range compression and registration, the mapping in (31) transforms the original range frequency variable f_r into the new range frequency variable, f_r'. By doing this, (31) can be expressed as:

$$\tilde{s}_{rc}(\tau, \eta) \approx T \cdot \text{sinc}(T(f_r - k_r\tau_0))$$
$$\cdot \exp\left(j\pi\left(2f_0\tau_0 - k_r\tau_0^2\right)\right) \quad (32)$$

At the end, we have a range-compressed signal with compensated phase error.

4 Experimental results

In this section, we demonstrate results of the proposed MC algorithm on both simulated and real FMCW data. The synthetic example is generated for point target, in which the simulation parameters for SAR system are given in Table 1.

Four different measures including sidelobe peak level ratio (SPLR), integrated sidelobe level ratio (ISLR), impulse response width (IRW), and 2D ISLR are used to evaluate the performance of different MC algorithms. SPLR is the ratio between the first sidelobe of the MF response and the peak of mainlobe. ISLR is the ratio between the returned energy of the mainlobe and that integrated over several (usually 10–20 dB) sidelobes on both sides of the main one. IRW is defined as the width of the mainlobe of the impulse response, measured 3 dB below the peak value. The 2D ISLR is similar to the 1D ISLR, with the main lobe defined within a rectangle with the size of the respective IRWs in each direction multiply by a constant (10 or more). The sidelobe power is then the power of the entire 2D image minus the main lobe power [20].

In the first experiment, a real flight GPS data are used to generate SAR raw signal for both point and distributed targets to validate the proposed MC algorithm. It should be mentioned that to better demonstrate the improvement using the proposed MC algorithm, the simulations are performed in noise-free condition. The results of traditional and proposed MC algorithms are shown in Fig. 4 for point target analysis.

It can be observed from the results that the proposed method outperforms the traditional MC algorithm in terms of resolution, sidelobes levels, and accuracy of targets locations. For point target analysis, azimuth and range slices of maximum points in the magnitude images are shown in Fig. 4, bottom row. From the results, one can see the improvements in the proposed motion compensation method as compared to the traditional algorithm [4]. In addition, the objective results of point target analysis are shown in Table 2. From

Table 1 SAR system parameters for raw data simulation

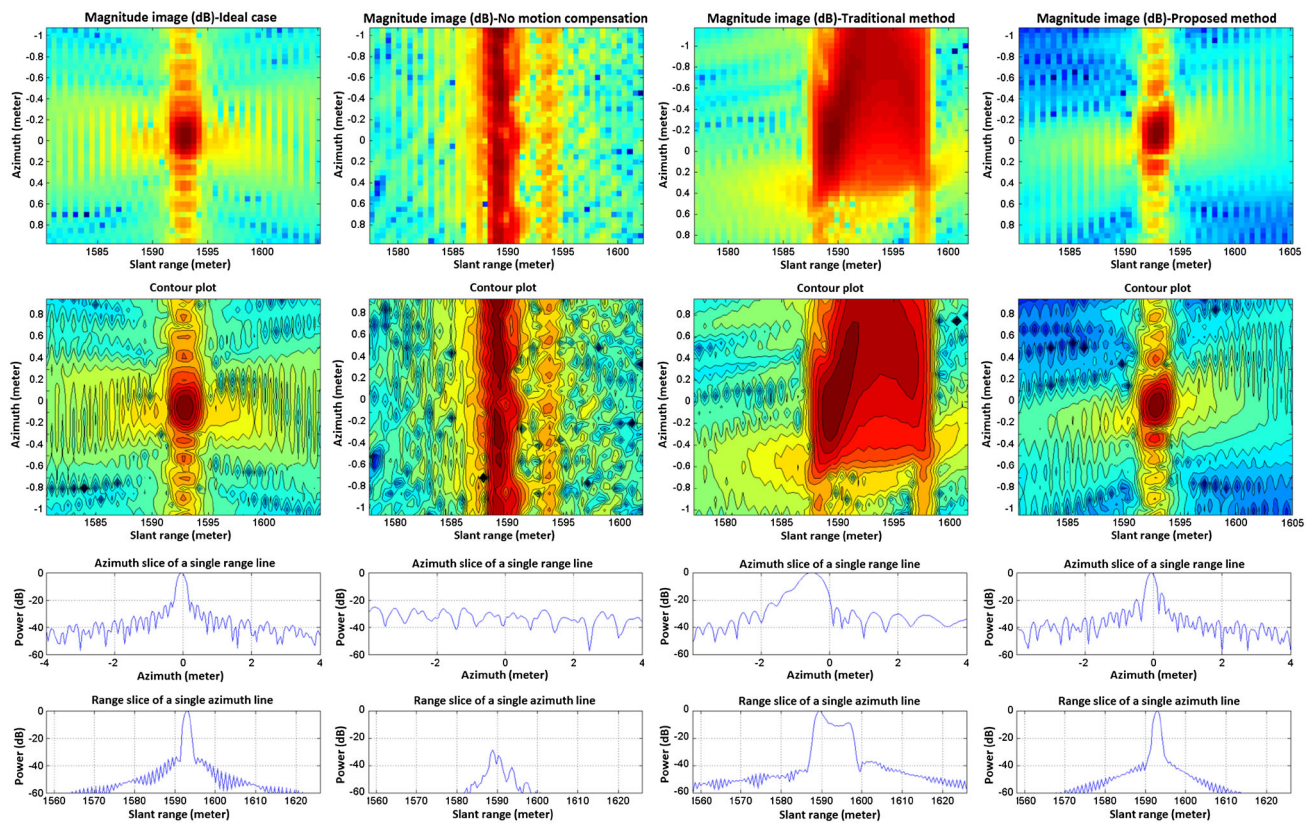| Parameter	Value
Velocity (m/s)	40
Bandwidth (MHz)	150
Pulse width (ms)	1.25
Swath width (m)	1200
PRF (Hz)	800
Altitude (m)	1300
Carrier frequency (GHz)	5.82
Sampling frequency (MHz)	3.2
Flight time (s)	8
Minimum range (m)	1338
Maximum range (m)	2000
Azimuth beamwidth (°)	8

Fig. 4 *Top row*, *left* to *right* amplitude image obtained in ideal case, without MC, traditional MC, and proposed MC. *Middle row* contour images of logarithmic scale for better visual comparison. *Bottom row* range and azimuth profiles for the point target in different conditions

Table 2 Results of MC experiment

Method	Ideal case	Traditional method [4]	Proposed method
SPLR$_{dB}$			
Range	−34.03	−26.95	−37.55
Azimuth	−21.67	−7.01	−24.20
ISLR$_{dB}$			
Range	−21.23	−23.78	−17.08
Azimuth	−10.84	−13.89	−10.81
2D ISLR$_{dB}$	−15.62	−19.82	−16.07
IRW$^*_{sample}$			
Range	2.49	3.56	2.47
Azimuth	3.79	9.51	3.84
Target position (m)			
Range	1593	1590	1593
Azimuth	0	−0.55	0

the results, it can be seen that for the proposed method, the target position accuracy and resolution are far better than the traditional algorithm.

In the second experiment, the raw SAR data with an imaging resolution of 1.5×1 m (range × azimuth) are collected by an experimental SAR, which was developed by the PARDIS electronic development company in Iran. A helicopter carried the SAR system. The experimental SAR system operated in C-band (5.20 GHz) with bandwidth 100 MHz. The helicopter flew at a height of about 200–1000 m, at a speed of 30–60 m/s. The return signal is amplified and mixed with the transmit signal. This de-chirped signal is filtered and then sampled with a 16 bit A/D at 8.33 MHz. The GPS provided motion information at the frequency of 10 Hz, and its positioning accuracy of GPS was 5 m. The images generated by the traditional and proposed navigation-based MC approaches are shown in Fig. 5c, d, respectively. The vertical direction is azimuth, and the horizontal direction is range. Apparently, it can be noted that the image generated by the traditional MC is blurred and distorted in geometry. While the image achieved by our approach is focused with a better quality. By compensating the spatially variant phases, the SAR imagery could be achieved with high precision. The local scene, highlighted in Fig. 5c, d by white rectangle, is amplified in Fig. 5 bottom row. There are groups of corner reflector arrays in the right corner of image. As clearly presented in the magnified image of Fig. 5d, the corner reflector arrays are focused in a good way. The presented algorithm was also tested in a sea area with a ship (see Fig. 6). In comparison, the magnified images of the scene highlighted by white rectangles are shown in Fig. 6 bottom row.

The shortcoming of the proposed MC method is the computationally taxing interpolation step as compared to the tra-
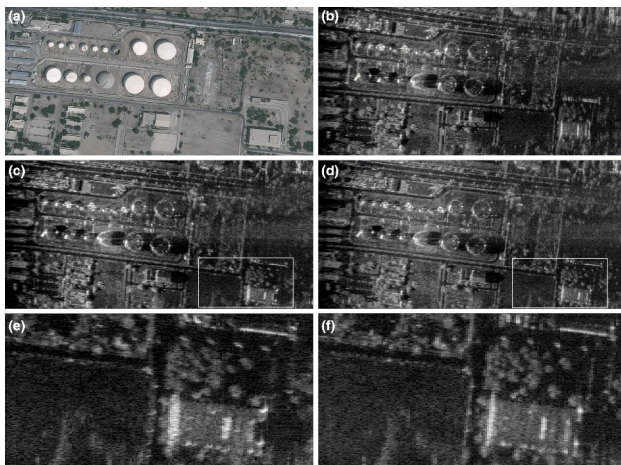
Fig. 5 a Aerial photograph of imaging area obtained from Google Earth. SAR data processed with the RDA (**b**) without MC, **c** traditional MC with navigation data, and **d** the proposed method. *Bottom row* magnified images highlighted by *white rectangles*
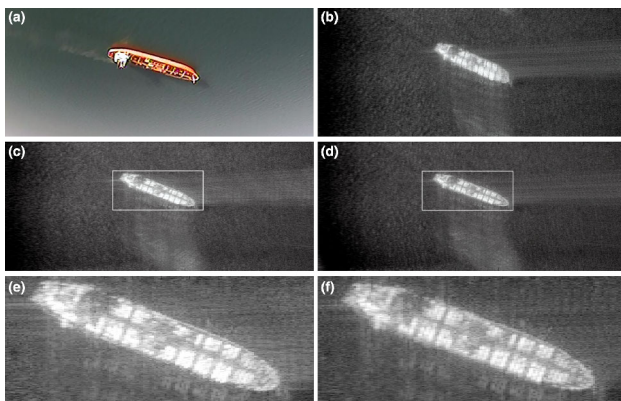

Fig. 6 a Aerial photograph of imaging area obtained from a camera mounted on the platform. SAR data processed with the RDA (**b**) without MC, **c** traditional MC with navigation data, and (**d**) the proposed method. *Bottom row* magnified images highlighted by *white rectangles*

ditional algorithm [4]. However, using the parallel nature of the algorithm and the parallel processing of modern general-purpose graphic processor units can significantly improve the processing time.

5 Conclusions

In this paper, the effects of non-ideal motion on an LFMCW SAR signal have been explored, and corrective algorithms have been developed. MC has successfully been applied to simulated and real SAR data by taking into account the motion during the chirp. The results show that it properly corrects the effects of non-ideal motion while offering some advantages. The proposed method can be implemented in place of the traditional method to improve processing efficiency and accuracy. The proposed algorithm is especially important when a SAR is operated on a small aircraft or UAS, which are especially susceptible to the effects of atmospheric turbulence. The results on real LFMCW SAR data show the validity of the proposed MC approach for RDA algorithm.

References

1. Mao, Y., Xiang, M., Wei, L., Horem, S.H.: The effect of IMU inaccuracies on airborne SAR imaging. J. Electron. (China) **28**(4–6), 409–418 (2011)
2. Horemuz, M., Andersson, J.V.: Polynomial interpolation of GPS satellite coordinates. GPS Solut. **10**, 67–72 (2006)
3. Gonzalez, P.J.T., Almorox, G.P., Burgos, G.M., Dorta, N.B.P.: SAR system for UAV operation with motion error compensation beyond the resolution cell. Sensors **8**(5), 3384–3405 (2008)
4. Kirk, J.C.: Motion compensation for synthetic aperture radar. IEEE Trans. Aerosp. Electr. Syst. AES-11 **3**, 338–348 (1975)
5. Meta, A., de Wit, J., Hoogeboom, P.: Development of a high resolution airborne millimeter wave FM-CW SAR. In: Proceedings of the First European Radar Conference, pp. 209–212 (2004)
6. Edrich, M.: Design overview and flight test results of the miniaturised SAR sensor MISAR. In: Proceedings of the First European Radar Conference, pp. 205–208 (2004)
7. Meta, A., Hakkaart, P., Zwan, F., Hoogeboom, P., Ligthart, L.: First demonstration of an X-band airborne FMCW SAR. In: Proceedings of the 6th European Conference on Synthetic Aperture Radar (2006)
8. Zaugg, E., Hudson, D., Long, D.: The BYU uSAR: A small, student-built SAR for UAV operation. In: Proceedings of the IEEE International Geoscience and Remote Sensing Symposium, pp. 411–414 (2006)
9. Edwards, M., Madsen, D., Stringham, C., Margulis, A., Wicks, B., Long, D.: MicroASAR: a small, robust LFM-CW SAR for operation on UAVs and small aircraft. In: Proceedings of the IEEE International Geoscience and Remote Sensing Symposium, vol. **5**, pp. 514–517 (2008)
10. Wang, W., Peng, Q., Cai, J.: Waveform-diversity-based millimeter wave UAV SAR remote sensing. IEEE Trans. Geosci. Remote Sens. **47**(3), 691–700 (2009)
11. Stevens, D.R., Cumming, I.G., Gray, A.L.: Options for airborne interferometric SAR motion compensation. IEEE Trans. Geosci. Remote Sens. **33**(2), 409–420 (1995)
12. Zaugg, E., Long, D.: Theory and application of motion compensation for LFM-CW SAR. IEEE Trans. Geosci. Remote Sens. **46**(10), 2990–2998 (2008)
13. Wang, R., Luo, Y.H., Deng, Y.K., Zhang, Z.-M., Liu, Y.: Motion compensation for high-resolution automobile FMCW SAR. IEEE Geosci. Remote Sens. Lett. **10**(5), 1157–1161 (2013)
14. Meta, A., Lorga, J.F.M., de Wit, J.J.M., Hoogeboom, P.: Motion compensation for a high resolution Ka-band airborne FM-CW SAR. In: IEEE European Radar Conference, pp. 1–4 (2005)
15. Meta, A., Hoogeboom, P., Ligthart, L.P.: Signal processing for FMCW SAR. IEEE Trans. Geosci. Remote Sens. **45**(11), 3519–3532 (2007)
16. Carrara, W.G., Goodman, R.S., Majewski, R.M.: Spotlight Synthetic Aperture Radar Signal Processing Algorithms. Artech House, Boston, MA (1995)
17. Franceschetti, G., Lanari, R.: Synthetic Aperture Radar Processing. CRC Press, Boca Raton, FL (1999)
18. Zaugg, E.: Generalized Image Formation for Pulsed and LFM-CW Synthetic Aperture Radar, Ph.D. Thesis (2010)
19. Cumming, G., Neo, Y.L., Wong, F.: Interpretations of the Omega-K algorithm and comparisons with other algorithms. Proc. IEEE Int. Geosci. Remote Sens. Symp. **3**, 1455–1458 (2003)
20. Cumming, G., Wong, F.H.: Digital Processing of Synthetic Aperture Radar Data Algorithms and Implementation. Artech House, Norwood, MA (2005)